

textured Au showed the relative change in the reflectance at >450 nm, which is in agreement with the observed color change in the Au plate.

Several studies have reported on the analysis of the optical properties of metal-filled anodic porous alumina; this material is typified as an array of metal particles in a dielectric medium, according to the Maxwell-Garnett and the Bruggman effective medium theory or the Mie-scattering theory (19–21). Our nanohole array of Au has an alternative structure: an array of air-filled holes in uniform metal. For this case the description for the inverted structure of the array of metal particles by Maxwell-Garnett theory has been reported to be applicable (22, 23). In the preliminary analysis of the experimental data, the qualitative shape of the reflectance spectra could be described by Maxwell-Garnett theory. For a qualitative analysis of the spectra, more detailed theories (23, 24) should be considered.

The process that we adopted may be useful in replacement studies of the nanostructures of other nanochannel materials (25, 26). Disadvantages, such as insufficient thermal and chemical stability or low mechanical strength that materials such as porous alumina might exhibit, might be overcome by this process. This nanochannel fabrication method should make it possible to fabricate nanocomposites with desired combinations of properties, a goal that has been difficult to accomplish with the conventional one-step host-guest embedding method.

REFERENCES AND NOTES

- B. Roxlo, H. W. Deckman, J. Gland, S. D. Cameron, R. Cianelli, *Science* **235**, 1629 (1987).
- K. Douglas, G. Devaud, N. A. Clark, *ibid.* **257**, 642 (1992).
- G. E. Possin, *Rev. Sci. Instrum.* **41**, 772 (1970).
- W. D. Williams and N. Giordano, *ibid.* **55**, 410 (1984).
- C. A. Huber *et al.*, *Science* **263**, 800 (1994).
- C.-G. Wu and T. Bein, *ibid.* **264**, 1757 (1994).
- F. Keller, M. S. Hunter, D. L. Robinson, *J. Electrochem. Soc.* **100**, 411 (1953).
- G. E. Thompson, R. C. Furneaux, G. C. Wood, J. A. Richardson, J. S. Gode, *Nature* **272**, 433 (1978).
- S. Kawai and R. Ueda, *J. Electrochem. Soc.* **122**, 32 (1975).
- M. Shiraki, Y. Wakui, T. Tokushima, N. Tsuya, *IEEE Trans. Magn.* **MAG-21**, 1465 (1985).
- M. Saito, M. Kirihara, T. Taniguchi, M. Miyagi, *Appl. Phys. Lett.* **55**, 607 (1989).
- C. J. Miller and M. Majda, *J. Am. Chem. Soc.* **107**, 3118 (1985).
- M. J. Tierney and C. R. Martin, *J. Electrochem. Soc.* **137**, 3789 (1990).
- T. Yoshino and N. Baba, *J. Chem. Soc. Jpn.* **1983**, 955 (1983).
- I. Mizuki, Y. Yamamoto, T. Yoshino, N. Baba, *J. Metal Surf. Finish. Soc. Jpn.* **38**, 561 (1987).
- H. Masuda, H. Tanaka, N. Baba, *Chem. Lett.* **1990**, 621 (1990); H. Masuda, K. Nishio, N. Baba, *Jpn. J. Appl. Phys.* **31**, L1775 (1992); *Thin Solid Films* **223**, 1 (1993); H. Masuda, T. Mizuno, N. Baba, T. Ohmori, *J. Electroanal. Chem.* **368**, 333 (1994).
- The Pt was deposited at 25°C with an electroless plating solution (PT-260, NE-CHEMCAT Company, Tokyo).
- The Au hole array was fabricated by electrochemical deposition of Au into the microcavity of the negative type of PMMA with an electroplating solution (ECF-60, NE-CHEMCAT) under the constant current condition of 4 mA cm⁻² at 22°C. The mother anodic alumina was formed at 17°C for 7 hours, the duration of the dipping treatment in phosphoric acid being 90 min. The hole depth was 3 μm. Although the defect-free domain size of the Au hole array is smaller than that of Pt hole array and had some distortion in regularity caused by the internal stress in the electrochemically deposited Au, the pore diameter and the interval of the Au hole array were almost the same as the values for the Pt hole array shown in Fig. 2.
- D. G. W. Goad and M. Moskovits, *J. Appl. Phys.* **49**, 2929 (1978); C. K. Preston and M. Moskovits, *J. Phys. Chem.* **92**, 2957 (1988).
- C. G. Granqvist, A. Andersson, O. Hunderi, *Appl. Phys. Lett.* **35**, 268 (1979).
- C. A. Foss Jr., G. L. Hornyak, J. A. Stokert, C. R. Martin, *J. Phys. Chem.* **98**, 2963 (1994).
- G. A. Niklasson and C. G. Granqvist, *J. Appl. Phys.* **55**, 3382 (1984).
- D. E. Aspnes, *Thin Solid Films* **89**, 249 (1982).
- G. B. Smith, *Appl. Phys. Lett.* **35**, 668 (1979).
- R. J. Tonucci, B. L. Justus, A. J. Campillo, C. E. Ford, *Science* **258**, 783 (1992).
- G. Widawski, M. Rawiso, B. Francois, *Nature* **369**, 387 (1994).

5 January 1995; accepted 13 April 1995

Lehmann Discontinuity as the Base of an Anisotropic Layer Beneath Continents

James B. Gaherty* and Thomas H. Jordan

Long-period surface-wave (R_1 , G_1), body-wave (S , SS , SSS), and ScS -reverberation data have been inverted to obtain anisotropic structures along seismic corridors that sample Australia and the western Pacific. These models support the proposal that the Lehmann discontinuity beneath stable continents represents a transition from an anisotropic lithosphere to a more isotropic material in the lower part of the continental tectosphere.

Lehmann (1) suggested that the behavior of refracted arrivals from North America and Europe at epicentral distances between 10° and 20° could be modeled by an increase in P -wave and S -wave speeds at a sharp lower boundary of the asthenospheric low-velocity zone (LVZ). Subsequent researchers argued that this Lehmann discontinuity (L) occurs globally at an average depth near 220 km (2, 3), and Dziewonski and Anderson (4) built this idea into the spherically averaged Preliminary Reference Earth Model (PREM). Solid-solid phase changes and chemical changes were ruled out as explanations (5), which led Hales (3) to conclude that this feature represents the base of a zone of partial melting, in agreement with Lehmann's basic hypothesis. However, L has not been detected in recent global stacks of long-period reflected waves (6), and, for a large area of the western Pacific and Australasia, it appears only on paths where the LVZ is weak or absent (7).

We have used new models of Australia and the western Pacific to test several alternative explanations of L that are based on the effects of seismic anisotropy. Leven *et al.* (5) proposed that L might be related to shear-induced anisotropy in the subcontinental mantle. From a structural model of the Australian upper mantle derived from refracted P waves, they hypothesized that L is the upper boundary of a thin plate-decou-

pling zone underlying a nearly isotropic continental mechanical boundary layer (Fig. 1A). Revenaugh and Jordan (7) obtained upper-mantle reflectivity profiles from vertically propagating ScS reverberations that indicated a ~2% increase in vertical shear (SV) impedance at an L with depths ranging from about 200 km along the northern Australian margin to more than 250 km beneath the Australian craton. Noting that the SV increase occurs near the level at which some studies of refracted SH waves in continents have found a shear-velocity decrease (8), they proposed an alternative model in which L marks the transition from an anisotropic mechanical boundary layer (MBL) to a more isotropic region below the MBL (Fig. 1B). On the basis of the apparent deepening of L toward the center of the western Australian craton, they speculated that this transition occurs at a critical temperature (near 1200°C) for the annealing of aligned textures in peridotites. They also pointed out that this horizon must be an internal feature of the continental thermal boundary layer, or tectosphere, whose thickness beneath cratons has been estimated to exceed 300 km (9).

Karato (10) accepted Revenaugh and Jordan's explanation of L as the rapid downward extinction of anisotropy, but he rejected their inference that such a feature could be maintained in a region with a low deformation rate internal to the tectosphere. Instead, he proposed that L represents the transition from dislocation-controlled creep to diffusion-controlled creep in an actively deforming asthenosphere beneath the con-

Department of Earth, Atmospheric, and Planetary Sciences, Massachusetts Institute of Technology, Cambridge, MA 02139, USA.

*To whom correspondence should be addressed.

tinental plate (Fig. 1C), and he reiterated Anderson's (2) suggestion that the tectospheric thicknesses obtained by Jordan (9) could be biased to high values as the result of anisotropic effects.

The models we have used to test these hypotheses were derived from seismic waves propagating within two corridors, one continental and one oceanic, chosen to minimize along-path heterogeneities arising from tectonic complications. The first is an Australian path, connecting earthquakes in the New Britain–New Guinea convergence zone with station NWAO, largely sampling the Phanerozoic platforms and Precambrian cratons of the Australian continent. The second is a Pacific path (11), connecting

earthquakes in the Tonga-Fiji seismic zone with stations in Hawaii, traversing oceanic lithosphere with an average age of about 100 million years. The reflectivity structures for the two corridors are quite different (12). We constrained the seismic velocities and their gradients by frequency-dependent travel times of turning (S, SS, and SSS) and surface (R_1 and G_1) seismic phases measured from three-component, long-period seismograms, using the isolation-filter techniques of Gee and Jordan (13). For the Australian corridor, we obtained approximately 800 observations for center frequencies from 10 to 45 mHz, using 20 events with epicentral distances from 37° to 44°.

We inverted the frequency-dependent

travel times and ScS reflectivity observations for a path-averaged, radially anisotropic model for each of the two corridors by means of an iterative, linearized perturbation scheme in which the elastic parameters, density, and discontinuity depths were adjusted to minimize a χ^2 measure of misfit (14). Our preferred Australia model (Fig. 2 and Table 1) achieved an 80% reduction in data variance relative to the isotropic starting model (Fig. 3, A through C). It is characterized by an anisotropic mantle above an L located at a depth of 252 ± 5 km and an isotropic mantle below this boundary. The transition from an anisotropic to an isotropic elastic structure at L is marked by an increase in SV impedance, consistent with the contrast observed for vertically propagating ScS reverberations. However, the model also shows a decrease in SH impedance at this transition, which indicates an SH low-velocity zone similar to those inferred for other continental regions (8). The density and mean values of the elastic parameters are almost continuous across L (Fig. 4A), as expected for a discon-

Fig. 1. Schematic cross sections of the continental upper mantle illustrating three competing hypotheses regarding the relation of L to upper-mantle anisotropy. **(A)** Model of Leven *et al.* (5), derived from an analysis of *P*-wave refraction data in northern Australia, which indicated a high-velocity zone in the depth interval from 190 to 225 km. They interpreted this feature to be an expression of the horizontal alignment of olivine crystals by the present-day northward motion of the Australian continent; L thus defines the transition between the base of the continental plate (tectosphere) and this narrow shear-decoupling zone. **(B)** Model of Revenaugh and Jordan (7), in which L is the base of an anisotropic MBL, overlying a nearly isotropic layer that forms the lower part of a thick (>300 km) continental tectosphere. The drop in the magnitude of the polarization anisotropy across this narrow (<30 km) transition causes an increase in the vertical wave speed and a decrease in the horizontal wave speed but no appreciable change in their isotropic average. **(C)** Model of Karato (10), who proposed that L is the transition from dislocation-dominated creep (which induces anisotropy in olivine) to diffusion-dominated creep (which does not) in an actively deforming asthenosphere beneath a thin (<200 km) continental tectosphere. The thickness of the shear-decoupling zone is not constrained in (B) or (C). Diagrams labeled $\Delta v/v$ show schematically the perturbations to the vertical (V) (solid line) and horizontal (H) (dashed line) wave speeds relative to the isotropic average; the left $\Delta v/v$ scale is for (A), and the right $\Delta v/v$ scale is for (B) and (C). In these diagrams, S is the free surface and M is the Mohorovičić discontinuity.

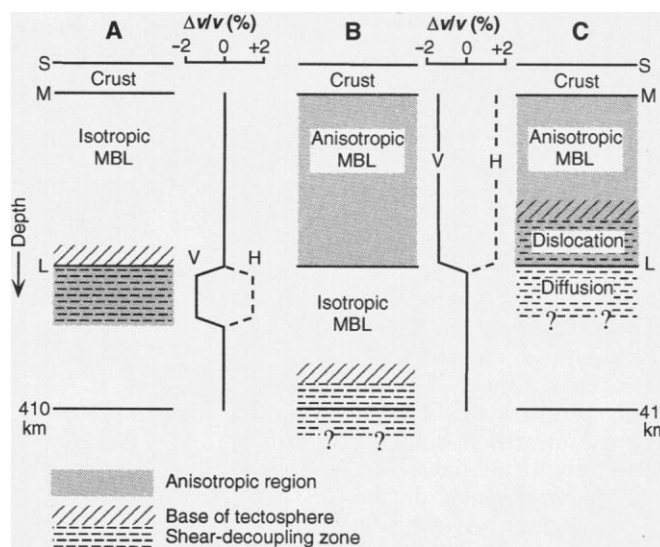


Fig. 2. Transversely isotropic model of the upper mantle for the Australian (New Britain–NWAO) corridor, obtained from the inversion of the 797 frequency-dependent travel times summarized in Fig. 3 and the 13 ScS reflectivity observations of (7). From left to right, the lines represent the anisotropic parameter η , density ρ , S-wave velocities v_{SV} and v_{SH} , and P-wave velocities v_{PV} and v_{PH} . Tick marks show the locations of the M, Hales (H), and L discontinuities; other first-order discontinuities are located at 406, 499, and 659 km. The model is radially anisotropic, with differing horizontal (dashed lines) and vertical (solid lines) velocities between M and L, and is isotropic elsewhere. The relative S-wave and P-wave anisotropies are comparable, averaging $3.3 \pm 0.5\%$ and $3.7 \pm 1.5\%$, respectively, although the former is much better determined by the data than the latter. The model is identical to PREM (4) below 860 km.

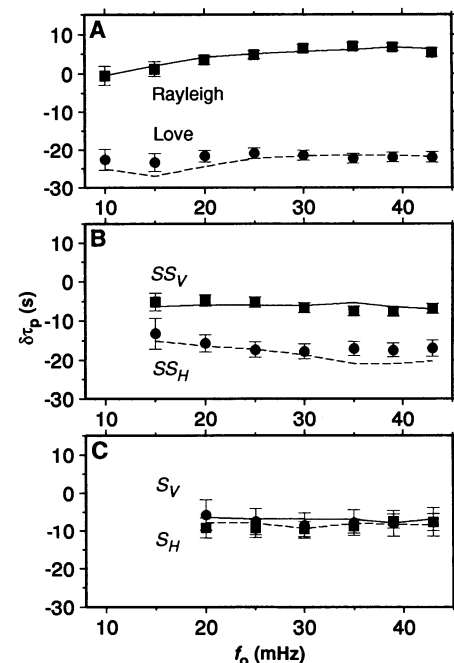
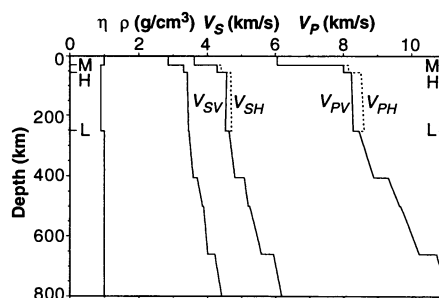


Fig. 3. Average phase delays $\Delta\tau_p$ for the Australian corridor, referenced to an isotropic starting model and plotted against circular frequency f_0 for surface waves **(A)**, SS waves **(B)**, and S waves **(C)**. Points with standard errors are averages of measurements for each seismic phase from vertical (■) and transverse (●) seismograms, summarizing the 797 frequency-dependent travel times used in the inversions; solid and dashed lines are corresponding averages computed for the Australia model of Fig. 2. The existence of polarization anisotropy at shallow depths in the Australian upper mantle is indicated by the large Love-Rayleigh discrepancy (>20 s), moderate SS-wave splitting (~10 s), and small S-wave splitting (<4 s).

tinuity that represents only a mechanical change in structure with no accompanying change in composition or phase.

We performed a number of inversions invoking a variety of prior constraints on the velocity distribution to test explicitly the hypotheses regarding the origin of L. The surface- and turning-wave data for the Australia corridor required significant radial anisotropy averaged over the upper 200 km of the mantle. Restricting the anisotropy to a thin (<100 km) layer near a depth of 200 km, as in Fig. 1A, resulted in models that did not satisfy the Love-Rayleigh discrepancy and SS splitting observations. On the other hand, the S and SS splitting data constrained the magnitude of the anisotropy below L to be small (<1%), and inversions that allowed anisotropy in the layer between L and the 410-km discontinuity yielded no significant improvement in the fit to the data relative to the preferred model of Fig. 2. The Australian data are therefore consistent with the idea that L is the base of the anisotropic layer.

To discriminate between the hypotheses illustrated in Fig. 1, B and C, we compared the shear-wave velocity structures derived for the Australian and Pacific corridors (Fig. 4A). The shear-wave anisotropy of the latter is similar in magnitude to that of the former and extends below the Gutenberg discontinuity (G) into the oceanic LVZ, terminating at a weak discontinuity (unresolved by the ScS reverberation data) at a depth of 170 km (11). Below G, however, the mean shear velocities are lower in the oceanic case, and this difference persists to depths greater than 350 km. Attempts to satisfy both the Pacific and the Australia data sets with models having similar shear velocities below 250 km were unsuccessful. Global tomographic models (15) and other regional studies (16) have demonstrated that differences between old continents and old oceans of this magnitude and depth are a global feature, indicative of

a thick tectosphere beneath most Precambrian continental shields and platforms (9, 17). We infer that the average thickness of the continental tectosphere beneath the Australia corridor is greater than 300 km, and we conclude that L is a transition internal to the tectosphere (Fig. 1B) rather than a boundary within an actively deforming asthenosphere beneath the continental plate (Fig. 1C).

This result implies that the anisotropy above L is frozen in an MBL, or lithosphere, that forms the cold upper part of the tectosphere. The anisotropy is most plausibly related to the lattice-preferred orientation of olivine, a highly anisotropic mineral known to dominate upper-mantle mineralogies (18). In the oceans, the fast axes of olivine grains tend to be horizontally aligned in the directions of the plate-scale flow associated with sea-floor spreading and are azimuthally coherent over large geographic distances. In the continents, however, the upper-mantle anisotropy appears to be inherited from major episodes of orogenic deformation (19). The superposition of many such episodes yields a fabric that varies on a much smaller geographical scale than the plate-tectonic flow field. In Australia, for example, lineaments in the gravity field associated with basement deformations have lateral scale lengths on the order of a few hundred kilometers (20). If this is the appropriate scale length for the decorrelation of the lattice-preferred orientation within the uppermost mantle beneath Australia, then waves propagating over epicentral distances of 30° to 40° will average out the azimuthal variations, and the path-averaged structure can be approximated by a transversely isotropic effective medium. This inference is consistent with data from earthquakes in the Banda Sea to station CAN in southeast Australia (Fig. 4B). Although these paths are orthogonal to those used in the inversion, we found that the Love-Rayleigh discrepancy and SS split-

ting measured for them were well fit by the Australia model.

As a further test, we developed stochastic models of upper-mantle heterogeneity in which orthorhombic periodotites have fast axes that are preferentially horizontal but randomly oriented in azimuth (21). At low frequencies, such models yield transversely isotropic effective media, and their radial anisotropy can be made to match the Australia data if local anisotropies derived from mantle xenoliths brought to the surface by kimberlite pipes are used (22). At high frequencies, strong multiple scattering from the anisotropic heterogeneities couples the SV and SH wave fields, thereby mixing the shear-wave polarizations; this scattering may explain why the apparent S_n speeds observed in western Australia on short-period, vertical-component seismograms (23) are consistent with our SH velocities and

Table 1. Upper-mantle model for Australia. Parameters are linearly interpolated between discontinuities. This model is identical to PREM (4) through the remainder of the lower mantle and core.

Depth (km)	V_{PH} (km/s)	V_{PV} (km/s)	V_{SH} (km/s)	V_{SV} (km/s)	ρ (g/cm ³)	η
0	6.05	6.05	3.62	3.62	2.85	1.00
30	6.05	6.05	3.62	3.62	2.85	1.00
30	8.15	8.00	4.40	4.28	3.30	0.90
54	8.15	8.00	4.40	4.28	3.30	0.90
54	8.52	8.23	4.68	4.56	3.40	0.90
252	8.61	8.28	4.70	4.52	3.44	0.90
252	8.45	8.45	4.63	4.63	3.45	1.00
406	8.88	8.88	4.80	4.80	3.58	1.00
406	9.31	9.31	5.07	5.07	3.69	1.00
499	9.64	9.64	5.19	5.19	3.85	1.00
499	9.67	9.67	5.23	5.23	3.88	1.00
659	10.21	10.21	5.58	5.58	4.00	1.00
659	10.72	10.72	5.94	5.94	4.21	1.00
861	11.21	11.21	6.28	6.28	4.50	1.00

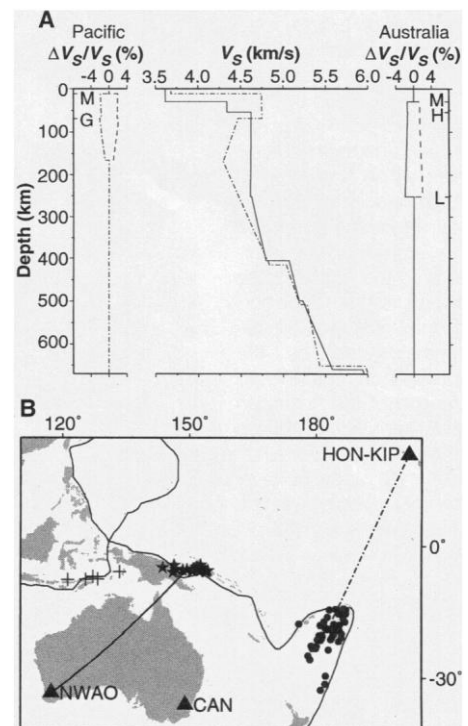


Fig. 4. (A) Comparison of shear-wave structures for the Australian and Pacific corridors. Mean shear-wave speeds are plotted for the Pacific (dashed-dot line) and Australia (solid line) in the center diagram, and the anisotropic velocity perturbations relative to these mean velocities are displayed on the left and right, respectively. The contrasts in velocities and discontinuity structure inferred above a depth of about 350 km are evidence for a thick tectosphere beneath Australia. (B) Location of earthquakes and seismic stations that define the two corridors. New Britain events (★) recorded at NWAO were used to generate the Australia model, and Tonga events (●) recorded at HON and KIP were used for the Pacific model. Banda Sea earthquakes (+) recorded at CAN were used to test for azimuthal variations in anisotropy beneath Australia.

not our SV velocities, and why paths that sample the upper 200 km of the northern margin of Australia do not show much S-wave splitting (24). The ScS reverberations, as well as the other data we used, cannot distinguish a sharp transition from a transition spread out over a depth interval of about 30 km (25). A transition zone of such width would explain why L is not consistently observed in studies of higher frequency converted waves (26).

The extinction of low-frequency polarization anisotropy at L can arise from either the disappearance of anisotropy at grain-size scales or the randomization of the fast-axis orientation out of the horizontal plane at regional scales. The first of these phenomena could be explained in terms of a kinetic boundary associated with long-term, thermally activated annealing of ancient deformation fabrics (27, 28) or, alternatively, by Karato's (10) rheological transition from dislocation to diffusion creep (although his proposal must be modified to generate an L that is a relic feature frozen into the continental tectosphere). The second could be caused by a depth variation in the types of strain fields active during tectospheric stabilization and any subsequent remobilization, for example, with deformations in the region above L involving nearly horizontal flows and those below L involving displacements with larger vertical components.

L is located near the maximum depth of equilibration (average ~220 km) observed for suites of kimberlite xenoliths from several continental cratons (29). This equilibrium level is interpreted to be the transition from slow diapiric upwelling of kimberlite magmas (or their precursors) (30) to much more rapid upward transport through a stronger lithosphere (31). L may thus correspond to the base of a mechanical boundary layer that overlies a more mobile, dynamically active part of the continental tectosphere. The apparent deepening of L beneath the western Australian craton (7) suggests that this rheological transition may be thermally controlled at 1200° to 1300°C. The transition also appears to correspond to a rapid increase in shear-wave attenuation observed at about this depth (32).

Our model provides an explanation for L in stable continental regions. Credible observations of discontinuities at depths of 180 to 220 km also have been made in island-arc (33) and marginal basin environments (7). Additional data will be needed to determine whether these discontinuities can be accounted for by the anisotropy-isotropy transition discussed here, or whether they require some other mechanism, such as the sharp lower boundary of a low-velocity zone. In this regard, Revenaugh and Sipkin (34) have recently invoked both mechanisms to explain the multiplicity of

discontinuities they observed in ScS reflectivity profiles crossing China and the Tibetan plateau.

REFERENCES AND NOTES

1. I. Lehmann, *Ann. Geophys.* **15**, 93 (1959); *Geophys. J. R. Astron. Soc.* **4**, 124 (1961).
2. D. L. Anderson, *J. Geophys. Res.* **84**, 7555 (1979).
3. A. L. Hales, *Geophys. J. Int.* **105**, 355 (1991).
4. A. M. Dziewonski and D. L. Anderson, *Phys. Earth Planet. Inter.* **25**, 297 (1981).
5. J. H. Leven, I. Jackson, A. E. Ringwood, *Nature* **289**, 234 (1981).
6. P. M. Shearer, *ibid.* **344**, 121 (1990).
7. J. Revenaugh and T. H. Jordan, *J. Geophys. Res.* **96**, 19781 (1991). This technique estimates the travel times down to and impedance contrasts across internal mantle reflectors from long-period, tangential-component recordings of multiple ScS reverberations. The ray paths of the reverberations are nearly vertical; hence, in the transversely isotropic model of mantle structure used here, the travel times and impedance contrasts are those defined in terms of the vertical shear (SV) velocities.
8. S. P. Grand and D. V. Helmburger, *Geophys. J. R. Astron. Soc.* **76**, 399 (1984); *Phys. Earth Planet. Inter.* **41**, 154 (1985).
9. T. H. Jordan, *Rev. Geophys.* **13**, 1 (1975).
10. S.-I. Karato, *Geophys. Res. Lett.* **19**, 2255 (1992).
11. J. B. Gaherty, T. J. Jordan, L. S. Gee, in preparation.
12. The Australian corridor was observed to have two reflectors in the mantle above 400 km, both characterized by impedance increases with depth: a Hales discontinuity (H) with an impedance contrast of $+4.9 \pm 0.9\%$ and a vertical S-wave reflection time of 28.4 ± 1.5 s, and an L with a contrast of $+2.1 \pm 0.6\%$ and a reflection time of 115.6 ± 1.0 s. The Pacific corridor featured a G with an impedance decrease of $-5.5 \pm 0.8\%$ and a reflection time of 29.7 ± 1.1 s, delineating the top of a relatively shallow (~60 km) S-wave low-velocity zone. Any G in Australia and any H or L in the Pacific were below the detection threshold of the ScS reverberation data, which is about 1%. As Revenaugh and Jordan have noted (7), H may well be a global feature associated with the spinel-garnet facies boundary that is obscured by G on this and some other oceanic paths. The migrated ScS reverberation data also showed systematic differences in the locations and amplitudes of the transition-zone discontinuities for the two corridors; the travel time between the 410- and 660-km discontinuities is greater for Australia, implying that temperatures are lower in the transition zone beneath the continent. We used these observations by directly incorporating the observed impedance contrasts and vertical reflection times as data in our inversions. We calculated the associated elements of the perturbation matrix with the use of ray theory and plane-wave reflection coefficients.
13. L. S. Gee and T. J. Jordan, *Geophys. J. Int.* **111**, 363 (1992). In this technique, an observed seismogram is cross-correlated with a synthetic wave group (the isolation filter), and the cross-correlogram is windowed in the time domain (to reduce interference from other wave groups) and narrow-band-filtered. To a good approximation, the resulting waveform is a Gaussian wavelet specified by four observables, which are functions of the narrow-band center frequency and functionals of the earth model. One of these generalized data functionals is the phase delay $\delta\tau_p$ of the observed wave group relative to the synthetic, that is, the frequency-dependent travel-time residuals used in this study. Gee and Jordan gave formulas for the Fréchet kernels of the phase-delay functional as a sum over traveling modes that include the first-order effects of interference from other arrivals. This methodology allowed us to consistently measure and interpret phase delays from complex wave groups such as SS and SSS on three-component seismograms without resorting to high-frequency or isolated-phase approximations.
14. In our models, the effective elasticity tensor was assumed to be transversely isotropic (radially anisotropic), parameterized according to the PREM conventions (4): v_{PH} and v_{PV} are the speeds of P waves propagating horizontally and vertically, respectively; v_{SH} is the speed of a horizontally propagating, transversely polarized shear wave; v_{SV} is the speed of a shear wave propagating either horizontally with vertical polarization or vertically with horizontal polarization; and η governs the variation of the shear and compressional wave speeds at oblique propagation angles. Between discontinuities, these five elastic parameters and the mass density ρ were taken to be linear functions of depth.
15. J. H. Woodhouse and A. M. Dziewonski, *J. Geophys. Res.* **89**, 5953 (1984); W.-J. Su, R. L. Woodward, A. M. Dziewonski, *ibid.* **99**, 6945 (1994).
16. S. P. Grand and D. V. Helmburger, *ibid.* **89**, 11465 (1984); A. L. Lerner-Lam and T. H. Jordan, *ibid.* **92**, 14007 (1987).
17. T. H. Jordan, in *Journal of Petrology, Special Volume*, M. A. Menzies and K. G. Cox, Eds. (Oxford Univ. Press, Oxford, 1988), pp. 11-37; _____, A. L. Lerner-Lam, K. C. Creager, in *Mantle Convection*, W. R. Peltier, Ed. (Gordon and Breach, New York, 1989), pp. 98-201.
18. L. H. Estey and B. J. Douglas, *J. Geophys. Res.* **91**, 11393 (1986); A. Nicolas and N. I. Christensen, *Rev. Geophys.* **25**, 111 (1987).
19. P. G. Silver and W. W. Chan, *J. Geophys. Res.* **96**, 16429 (1991); P. G. Silver and S. Kaneshima, *Geophys. Res. Lett.* **20**, 1127 (1993).
20. See figure 1.1 of R. W. R. Rutland, in *Precambrian of the Southern Hemisphere*, D. R. Hunter, Ed. (Elsevier, Amsterdam, 1981), p. 5.
21. T. H. Jordan and J. B. Gaherty, in *Proceedings of the 16th Annual Seismic Research Symposium*, J. J. Cipar, J. F. Lewkowicz, J. M. McPhetres, Eds. (Phillips Lab. Tech. Rep. PL-TR-94-2217, Hanscom Air Force Base, MA, 1994), pp. 189-195. In these stochastic models, the spatial distribution of orientations is scale-invariant (fractal) up to some horizontal correlation length (outer scale) ℓ_o , and some vertical correlation length ℓ_z . We distinguish two cases: equidimensional stochastic heterogeneity, with an aspect ratio near unity ($a \equiv \ell_o/\ell_z \sim 1$), and a stochastic laminate, with a large aspect ratio ($a \gg 1$). For wavelengths much greater than ℓ_z and propagation distances much greater than ℓ_o , the effective media in both cases are transversely isotropic with elastic properties that are independent of ℓ_o and ℓ_z .
22. The local anisotropy measured in mantle xenoliths ranges from 3 to 8% [(28); N. I. Christensen, personal communication]. The relative shear-wave anisotropy of 3% obtained for Australia can be made consistent with these somewhat larger values if we invoke dispersion of the fast (a) axis of olivine out of the horizontal plane.
23. J. R. Bowman and B. L. N. Kennett, *Bull. Seismol. Soc. Am.* **83**, 25 (1993).
24. C. Tong, O. Gudmundsson, B. L. N. Kennett, *J. Geophys. Res.* **99**, 15783 (1994).
25. See figure 4 of J. Revenaugh and T. H. Jordan, *ibid.* **96**, 19763 (1991).
26. G. Bock, *Geophys. J.* **94**, 73 (1988).
27. A. M. Boullier and A. Nicolas, *Phys. Chem. Earth* **9**, 467 (1975).
28. D. Mainprice and P. G. Silver, *Phys. Earth Planet. Inter.* **78**, 257 (1993).
29. A. A. Finnerty and F. R. Boyd, in *Mantle Xenoliths*, P. H. Nixon, Ed. (Wiley-Interscience, Chichester, UK, 1987), pp. 381-402.
30. H. W. Green II and Y. Gueguen, *Nature* **249**, 617 (1974).
31. D. A. Spence and D. L. Turcotte [J. Geophys. Res. **95**, 5133 (1990)] argued that kimberlites erupt by magma fracture, which implies a mechanically competent lithosphere extending to their depths of origin.
32. O. Gudmundsson, B. L. N. Kennett, A. Goody, *Phys. Earth Planet. Inter.* **84**, 207 (1994).
33. J. E. Vidale and H. M. Benz, *Nature* **356**, 678 (1992).
34. J. Revenaugh and S. A. Sipkin, *J. Geophys. Res.* **99**, 21911 (1994).
35. We thank L. Gee and S. Shapiro for assistance in code development during the early stages of this project and P. Shearer for a helpful review of the manuscript. Sponsored by the Air Force Office of Scientific Research under grant F49620-92-J0404.

4 January 1995; accepted 23 March 1995